M. Contreras, M.I. Martín, M.J. Gázquez, M. Romero, J.P. Bolívar. Valorisation of ilmenite mud waste in the manufacture of comercial Ceramic. *Construction and Building Materials* 72 (2014) 31–40; doi:10.1016/j.conbuildmat.2014.08.091

Valorisation of ilmenite mud waste in the manufacture of commercial ceramic

M. Contreras[a], M.I. Martín[b, 1], M.J. Gázquez[a], M. Romero[b], J.P. Bolívar[a]

[a] Departamento de Fisica Aplicada, Universidad de Huelva, Campus de Excelencia Internacional del Mar (CEIMAR), 21071 Huelva, Spain

[b] Grupo de Materiales Vítreos y Cerámicos, Departamento de Construcción, Instituto de Ciencias de la Construcción Eduardo Torroja IETcc-CSIC, 28033 Madrid, Spain

Abstract

This paper reports the results of a study focused on the production of ceramic tiles from ilmenite mud (MUD), a waste generated by the industry devoted to the TiO_2 pigment production. Ceramic tiles were produced from mixtures of a commercial red stoneware mixture (RSM) with different concentrations of mud (3, 5, 7, 10, 30 and 50 wt.%). The samples were sintered to simulate a fast-firing process. The sintering behaviour of the fired samples was evaluated according to ISO methodologies by linear shrinkage, water absorption and porosity measurements. Both green powder and fired samples were characterised by means of X-ray diffraction (XRD), differential scanning calorimetry (DSC/TG), field emission scanning electron microscopy (FESEM) and bending strength measurements. Moreover, since this activity is a NORM (Naturally Occurring Radioactive Material) industry, the radionuclides activity concentrations were measured by both gamma and alpha spectrometry techniques. Finally, the TCLP leaching test (Toxicity Characteristic Leaching Procedure, USEPA) was performed to assess the risks of the use of undissolved mud tiles from an environmental perspective. The results obtained demonstrated that ilmenite mud can be successfully valorisated in the manufacture of red stoneware ceramic bodies, with even better technological properties than commercial ones. The addition of mud as additive (from 3% to 10%) had a beneficial effect to the sintering processes, improving the bending strength (up to 15%) and reducing both apparent porosity and water absorption (up to 50%).

Keywords Ceramic tile; NORM waste; Ilmenite mud; Red stoneware; Valorisation

M. Contreras, M.I. Martín, M.J. Gázquez, M. Romero, J.P. Bolívar. Valorisation of ilmenite mud waste in the manufacture of comercial Ceramic. *Construction and Building Materials* 72 (2014) 31–40; doi:10.1016/j.conbuildmat.2014.08.091

1. Introduction

Because of the depletion of natural resources, increasing greenhouse emissions and awareness of the need for sustainable development in terms of safe reuse of wastes, the transformation of these wastes into valuable materials (i.e. valorisation) is emerging as a strong trend. In this context and taking into account the growing awareness of the need for protection of health and environment, the recovery of wastes currently generated in most industrial processes is the subject of a thorough investigation [1], [2] and [3]. The valorisation of wastes as secondary raw materials in the manufacture of construction materials could allay the problems associated with both the depletion of natural resources and the disposal of industrial wastes [4], [5], [6] and [7]. In this context the protection of health and environment is of great importance, although the economic benefits accruing from waste recycling must not be ignored [8] and [9].

This work is mainly focused on the recovery of waste generated by the titanium dioxide pigment industries. TiO_2 production begins with the mixing of ilmenite (Fe_2TiO_3) with highly concentrated sulphuric acid (80–95%) [10]. The liquor generated goes to a clarification tank where the un-attacked solid – ilmenite mud (MUD) – is allowed to settle. Then this mud is separated from the liquor by a process of decantation and filtration, and finally stored in a safety area. The magnitude of this generated waste is around 30,000 tons per year, which until now have not had any use, and therefore it is disposed of in an authorised waste repository [11]. Moreover, the content of natural radionuclides is high in relation to a typical soil (about 100 times higher), and so it is classified as a NORM (Naturally Occurring Radioactive Material) industry, which presents enhanced levels of radionuclides from the natural uranium and thorium series.

This waste has been classified by the competent authorities as “hazardous waste”, according the European legislation (Commission Decision 2000/532/EC as amended three times by the Commission Decisions 2001/118/EC, 2001/119/EC and 2001/573/EC). Therefore now this is stored in a controlled landfill repository, which implies a cost of about three million euros for its final elimination (including transportation costs). Therefore, if this waste could be valorised a significant improving in the competitiveness of this industry will be produced.

In this context, a correct environmental solution to the disposal of a wide range of solid wastes could be their incorporation into ceramics [12] and [13]. The prospective benefits of using ilmenite mud as an additive in tile manufacture include immobilising some heavy metals and radionuclides in the final matrix, oxidising organic matter and destroying any pathogens

during the firing process, as well as reducing frost damage, based on the results of several full- or bench-scale studies [14], [15] and [16]. In addition, there is no costs in incorporating this waste like additive in ceramics production, depending the saving on the fraction of waste added to each tile and the costs of the transportation of the waste from into the ceramic plant. Therefore, as average we think that no additional costs will be involved in the use of this waste for ceramic manufacturing.

Taking into account the mud's composition [16], [17] and [18], it is essential to study whether the presence of this residue modifies the mechanical properties of the new ceramic tile through a physico-chemical analysis (elemental, mineralogical and morphological) of the wastes and raw materials used in the generation of the tile tested. In addition, it is essential to check its environmental impact in relation to the potential problem of leaching of metals and radionuclides included in the ceramic matrix.

Taking in consideration the previously established problem, the main objective of this work was to analyse the option of producing ceramic tiles with different ilmenite mud waste proportions and compare it with a standard commercial ceramic, studying its technological properties and the environmental implications.

2. Materials and methods

2.1. Materials and sample preparation

The ilmenite mud was previously dried in an oven at 110 °C for at least 48 h until constant weight, and then grounded and sieved to a particle size >160 μm. As it will be discussed further, the ilmenite mud is characterised by a high content of iron oxide (Fe_2O_3 = 10%). For that reason, its valorisation in ceramic tile has been achieved through its incorporation into a composition of red stoneware, which is made from natural clays with high iron oxide content (Fe_2O_3 > 7%). Several mixtures with red stoneware (RSM [code sample 100/0]; supplied by Tierra Atomizada, S.A.) and different concentrations of ilmenite mud (3%, 5%, 7%, 10%, 30% and 50%, code samples 97/3, 95/5, 93/7, 90/10, 70/30 and 50/50 respectively) were prepared. The mixtures moistened by spraying with distilled water (6 wt.%) and then shaped by uniaxial pressing (Nannetti S hydraulic press) at 40 MPa in a steel die, to obtain tiles measuring 50 × 50 × 5 mm. These tiles were fired in an electric furnace at 1150 °C for eight minutes following the fast-firing process recommended by the red stoneware supplier (Fig. 1).

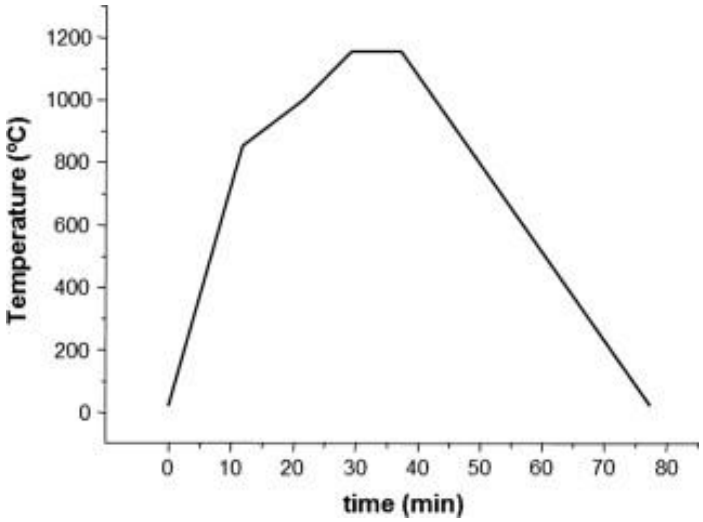

Fig. 1. Heating cycle used for the fast-firing of ceramic tiles

2.2. Characterisation techniques

The identification of the mineral phases was performed by the XRD technique (X-ray diffraction) which applied the method of dust lost in a Bruker diffractometer (model D8 Advance), using Cu Kα radiation excited by a current of 30 mA and a voltage of 40 kV. Data were recorded in the 5–70° 2θ range (step size 0.019736° and 0.5 s counting time for each step).

The measurement of major elements and trace elements was performed by ICP-MS (Inductively Coupled Plasma Mass Spectrometry), using an HP branded computer model HP4500® and by ICP-OES (Inductively Coupled Plasma Optical Emissions Spectrometer) using a Jobin Yvon ULTIMA 2. Both systems were previously calibrated with the appropriate standards.

The microstructure of tiles was examined by field emission scanning electron microscopy (FESEM) (HITACHI model S-4800) operating at 20 kV. SEM specimens were polished with 6, 3 and 1 μm diamond pastes after grinding with silicon carbide paper and water and subsequently Au–Pd coated in a Balzers SCD 050 sputter.

The thermal behaviour of the raw materials (ilmenite mud and RSM) and all the mixtures were evaluated by differential scanning calorimetry (DSC) and thermogravimetric analysis (TGA) (SETARAM model Labsys) on powder samples (size particle = 80–100 μm). DSC/TGA scans were performed between 25 °C and 1450 °C at 50 °C/min in flowing air, platinum crucibles and calcined Al_2O_3 as reference material. The DSC/TG curves were normalised regarding the sample weight.

2.3. Technological characterisation

The sintering behaviour of tiles was evaluated on the basis of water absorption, apparent porosity and bulk density. The water absorption was measured according to EN ISO 10545-3 [19] for ten representative specimens. The water absorption coefficient, *E* (dry wt.%), was calculated by the equation:

$$E = [(_{m2} - _{m1})/_{m1}] \times 100 \quad (1)$$

where m_2 (g) is the mass of wet specimen and m_1 (g) is the mass of dry specimen.

The apparent porosity and the bulk density were measured according to ASTM C373-88[20], which involves drying the test specimens to constant mass (*D*). The test was carried out on ten representative specimens. After impregnation, the mass (*S*) of each specimen while suspended in water and their saturated mass (*M*) was determined. The apparent porosity, *P* (%), expresses the relationship of the volume of open pores with the exterior volume of the specimen and is calculated as follows:

$$P = [(M - D)/(\rho \cdot V)] \times 100 \quad (2)$$

where V (cm^3) is the exterior volume ($V = M - S$) and ρ is the density of the water 1 g cm^{-3}.

The bulk density, B (g cm^{-3}), of a specimen is the quotient of its dry mass divided by the exterior volume, including pores:

$$B = D/V \quad (3)$$

Linear shrinkage, LS (%), was calculated by the equation:

$$LS = (_L i - _L f) \times 100/_L i \quad (4)$$

where L_i (mm) is the specimen length without firing and L_f (mm) is the specimen length after firing.

Bending strength, BS (MPa), was measured according to EN 843-1 [20] in an electronic universal tester (Servosis model ME-402/01) on ten test specimens for each sintered temperature by a three-point loading test with a span of 32 mm and a crosshead speed of 1 mm/min.

2.4. Radioactive characterisation of materials and mixtures obtained

The activity concentrations of radionuclides in the ilmenite mud were measured by high-resolution low-background gamma spectrometry with high-purity germanium detectors (HPGe).

In addition, the concentrations of both Th-, U-isotopes and ^{210}Po were determined by the alpha spectrometry technique with ion-implanted Si detectors (PIPS detectors) [21].

On the other hand, the radon potential (Ω) is defined as the ^{222}Rn concentration generated inside the material from the ^{226}Ra contained inside it that can be transported through its pores, and it is calculated by multiplying the ^{226}Ra concentration (Bq kg^{-1}) for the radon emanation factor (ε). The method for measuring Ω is described in López-Coto et al. [22], which is determined from the growth curves of radon inside a closed chamber it is possible to calculate the exhalation rate of the block and, under specific experimental conditions, the radon potential of the tested material.

2.5. Pollutant mobility tests

To assess the risks of the use of a waste, from an environmental perspective, the TCLP leaching test (Toxicity Characteristic Leaching Procedure, U.S. EPA) was carried out [23]. The pollutant concentrations in the leaching dissolutions obtained from the mobility tests were analysed by ICP-OES and ICP-MS. In addition, the concentrations of different radionuclides contained in the leaching dissolutions were analysed by both alpha and gamma spectrometry techniques.

3. Results and discussion

3.1. Physico-chemical characterisation

3.1.1. Mineralogy

In previous works [24], the ilmenite mud has shown to be composed by several major mineral species such as ilmenite ($FeTiO_3$), rutile (TiO_2) and anatase (TiO_2), and containing other minor mineral phases: zircon ($ZrSiO_4$), quartz (SiO_2) and Fe and Ti oxides ($Fe_3Ti_3O_{10}$). On the other hand, the RSM showed as main mineral phases kaolinite ($Al_2Si_2O_5(OH)_4$) and illite ($KAl_2Si_4O_{10}(OH)_2$), with traces of quartz (SiO_2), anorthite ($CaAl_2Si_2O_8$), rutile (TiO_2) and hematite (Fe_2O_3) [25] and [26].

In Fig. 2 can be observed that, after the firing process, the peaks associated with clay minerals (kaolinite and illite) disappear because of the destruction of the crystalline structure at 450–900 °C. Finally, at 1000 °C the feldspars (anorthite) undergo melting and form liquid phases [27]. In our case the potassium oxide released by illite favoured the agglomeration of the particles [28]. The minerals detected, included ilmenite, rutile and anorthite, increased in the ilmenite mud concentration, whereas the peaks of quartz decreased in the ceramic body (Fig. 2).

Ilmenite mud has an important content of iron and titanium oxides, which are known as nucleating agents that promote the crystallisation of mineral phases like the anorthite [29].

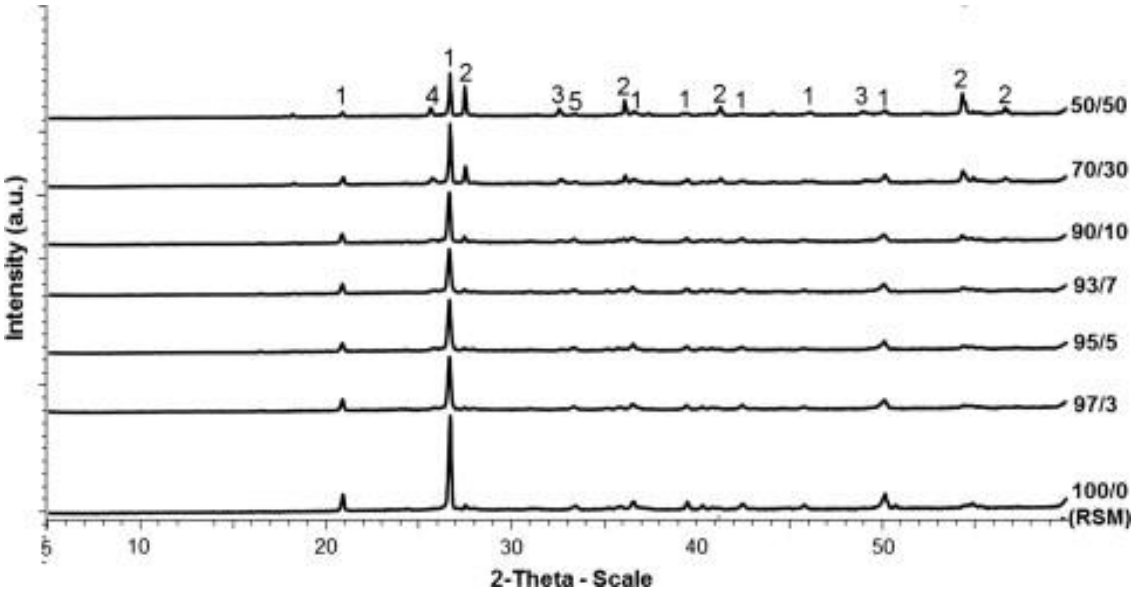

Fig. 2. XRD patterns of fired tiles. [1]: quartz (SiO_2); [2]: rutile (TiO_2); [3]: ilmenite ($FeTiO_3$); [4]: anorthite ($CaAl_2Si_2O_8$) and [5]: Ti and Fe oxides ($Fe_3Ti_3O_{10}$).

3.1.2. Chemical analysis

Ilmenite mud shows a high content of TiO_2 (56 wt.%), SiO_2 (18 wt.%), Fe_2O_3 (10 wt.%) and Al_2O_3 (5.1 wt.%) (Table 1) as expected [11]. Moreover we found 2.96 wt.% of SO_3, predictable because the ilmenite mud is produced by sulphuric acid digestion. It is also observed a high concentration in other elements as Zr (2.3 wt.% of ZrO), according to the mineralogical composition.

Table 1. Concentrations of majority (wt.%) and trace (mg kg^{-1}) elements in the raw materials used in the manufacturing process of the tiles.

RSM/MUD	Major Elements										Trace Elements						
	Al_2O_3	CaO	Fe_2O_3	K_2O	MgO	Na_2O	SO_3	SiO_2	TiO_2	ZrO_2	As	Ba	Cr	Mn	Pb	Sr	Zn
MUDa	5.12	1.11	10.37	1.29	1.33	1.02	2.60	18.43	56.43	2.30	<3	480	901	1910	282	130	177
0/100 (MUDb)	5.95	1.54	10.32	1.27	1.38	1.05	0.05	18.23	57.73	2.47	13	785	500	2030	281	135	183
RSMa	19.94	2.10	7.39	4.20	1.73	0.58	0.06	62.00	1.67	0.32	10	568	69	338	39	108	268
100/0 (RSMb)	21.30	2.09	9.04	4.25	1.76	0.61	0.06	58.88	1.67	0.32	9	601	71	447	58	116	279
90/10	20.73	1.98	9.66	4.12	2.73	0.70	0.06	52.94	6.62	0.47	<3	594	129	575	68	113	268
50/50	13.78	1.68	10.30	2.94	1.66	0.93	0.15	39.01	28.22	1.34	<3	737	319	1300	182	129	234

a Before firing process.
b After firing process.

The RSM analysis reported SiO_2 (62 wt.%), Al_2O_3 (20 wt.%), Fe_2O_3 (7.4 wt.%), K_2O (4.2 wt.%) and CaO (2.1 wt.%). The trace elements (As, Ba, Cr, Mn, Pb, Sr and Zn) were present at concentrations below 0.1%. Comparing the raw materials before and after firing, we found that most values were practically identical, with the exception of sulphur in mud samples, whose concentration decreased from 2.60% to 0.05% because of volatilisation during the firing process, fact expected since S could be released during the firing as sulphur oxide (SOx).

If for a specific element is supposed a conservative behaviour during the firing, its concentration (C) in the final mixture (manufactured by the 1 and 2 components), will be given by the equation $C = (C1 - C2)\cdot x + C2$, where $C1$ and $C2$ are the concentrations of the element in the respective components. Therefore, if these concentrations have been experimentally measured, a very good linear fitting has to be found between "C" and proportion (X) of a specific component of the mixture. In general, very high determination coefficients ($R^2 > 0.99$), were obtained for the majority of the elements analysed, validating internally the measuring methods of the chemical and radioactive analysis. For example, the obtained fitting to ^{228}Ra was the following: C (Bq kg^{-1}) = (67 ± 7) + (8.85 ± 0.17) X(R^2 = 0.9986), X in %.

The location of tested compositions in the SiO_2–Al_2O_3–TiO_2 and SiO_2–Al_2O_3–Fe_2O_3 ternary systems is shown is Fig. 3. As expected, the high TiO_2 content in the composition of ilmenite mud waste leads to ceramic compositions highly dispersed in the diagram SiO_2–Al_2O_3–TiO_2. In contrast, the iron oxide contents in both ilmenite mud and RSM composition are quite similar, giving rise to ceramic compositions converged in a narrow area of the corresponding diagram, around 7.5–9% of Fe_2O_3.

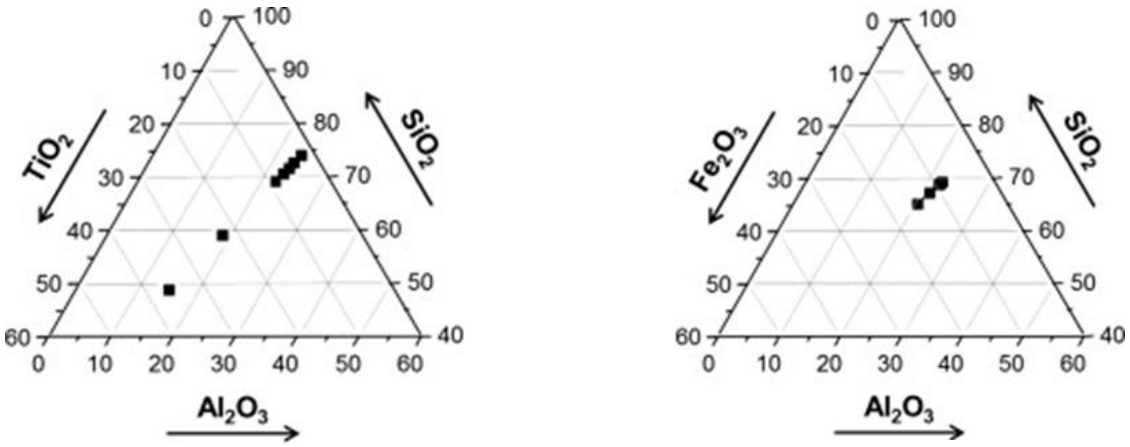

Fig. 3. Location of tested composition in the SiO_2–Al_2O_3–TiO_2 and SiO_2–Al_2O_3–Fe_2O_3 ternary systems.

3.1.3. DSC/TGA

The thermal behaviour of the main materials was studied trough the DSC/TG curves (Fig. 4). The losses on ignition (1150 °C) are 9.60 wt.% and 8.25 wt.%, for ilmenite mud and RSM respectively. The red stoneware composition shows six areas of weight change. The first one at ~100 °C corresponds to the endothermic evaporation of unbound water. The second area (between 200 and 500 °C), is associated with the thermal decomposition of non-volatile organic compounds, the exothermic combustion of non-volatile organic matter and the endothermic volatilisation of lighter organic fragments. The third area at ~600 °C is related to the thermal destabilisation of hydrated minerals and the release of crystallisation water. The fourth area ~800 °C is associated with the decomposition of alkaline compounds. The fifth area ~900 °C is associated with the decomposition of alkaline-earth carbonates and the release of carbon dioxide. Finally, an endothermic descent at higher temperatures indicates the formation of a liquid phase mainly derived from the feldspar component and silica release [30].

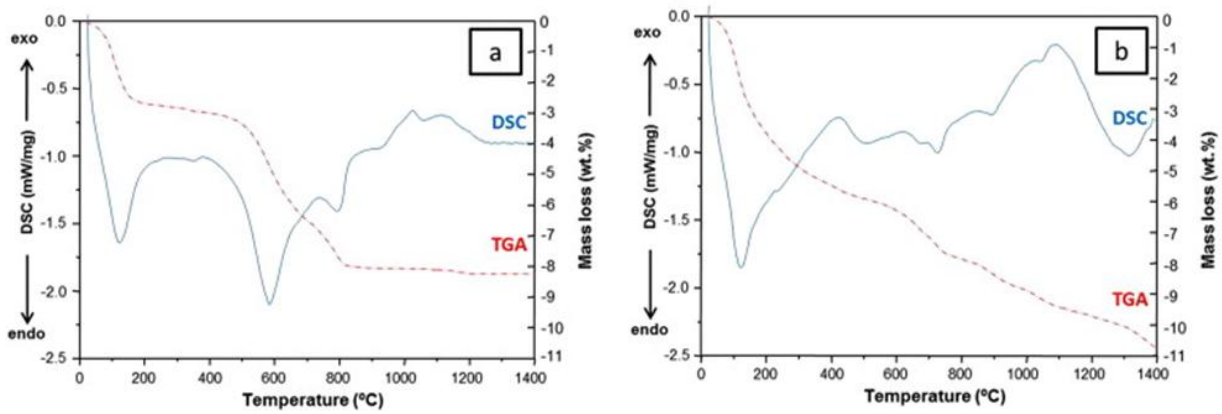

Fig. 4. DSC/TG curves (25–1450 °C, 50 °C/min); (a) RSM and (b) tionite.

The thermal behaviour of ilmenite mud shows five primary effects (Fig. 4). The first one is related to the endothermic loss of the chemically bound water of $FeSO_4 \cdot xH_2O$ at ~110 °C. The next areas can be attributed to $Fe_2(SO_4)_3$. The second area appears at ~550–600 °C, the loss weight produced by the thermal decomposition of $FeSO_4$, associated with an endothermic reaction. The third area ~700 °C is associated with the decomposition of $Fe_2(SO_4)_3$ into Fe_2O_3 and the fourth area ~850 °C corresponds to the loss of weight produced by the decomposition of calcium and potassium carbonate that is present at high concentrations in the ilmenite mud. Finally, an endothermic descent at higher temperatures indicates the formation of

amorphous silica released during decomposition; the impurities contained in the raw materials could also contribute to a liquid phase formation [31].

According the thermal behaviour of the mixtures given by the TG curves (Fig. 5), the losses on ignition (1150 °C) are between 9.75 wt.% and 7.30 wt.% (see Table 2). The samples have almost no loss on ignition. The thermal behaviour of each mixtures given by the DSC curves (Fig. 6), are quite similar to the red stoneware, especially those that exhibit the greatest proportion of RSM (Fig. 6a–c). In samples that contain at least 10% in tionite, this similar thermal behaviour changes and appears new areas associated with the thermal behaviour of ilmenite mud. Fig. 6d–f shows these new areas where both thermal behaviours converge. The first area at ~100 °C corresponds to the endothermic evaporation of unbound water in RSM, but also appear in these cases the area related to the endothermic loss of the chemically bound water of iron sulphate (II) and the decomposition of $FeSO_4 \cdot xH_2O$ at ~110 °C in ilmenite mud. Moreover, this same fact happens with the other different areas at ~500–900 °C in which the thermal behaviour of both materials appears but less clear than in the previous case.

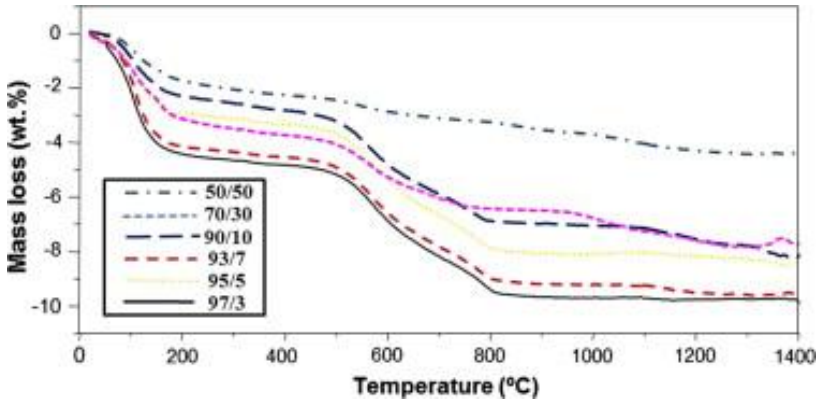

Fig. 5. TG curves (25–1450 °C, 50 °C/min) of 97/3, 95/5, 93/7, 90/10, 70/30 and 50/50.

Table 2. Loss in ignition (wt.%) of main materials and the different mixtures samples obtained by the DSC/TGA curves.

RSM/MUD	Loss in ignition
100/0 (RSM)	8.25
97/3	9.75
95/5	8.12
93/7	9.25
90/10	7.30
70/30	7.45
50/50	8.25
0/100 (MUD)	9.60

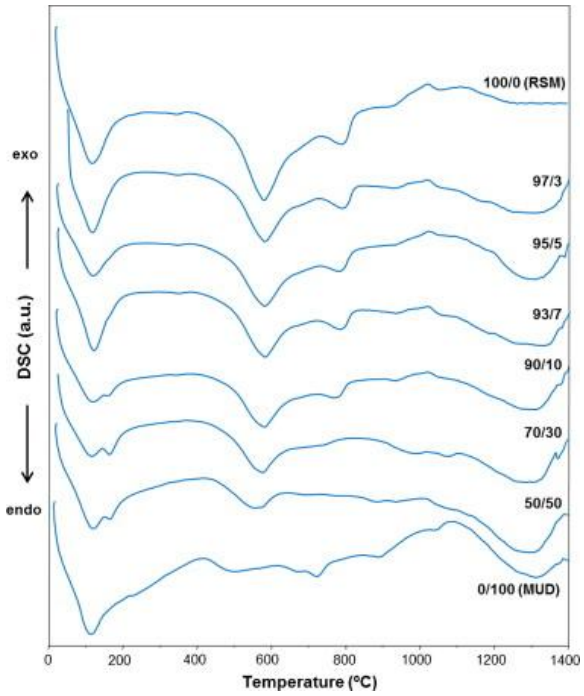

Fig. 6. DSC curves (25–1450 °C, 50 °C/min); (a) 97/3, (b) 95/5, (c) 93/7, (d) 90/10, (e) 70/30 and (f) 50/50.

3.1.4. Field emission scanning electron microscopy (FESEM)

In order to analyse how the undissolved mud was incorporated in the final product, a detailed study by FESEM (Fig. 7) on polished surfaces of fired samples was made. In all cases, after firing the ceramic bodies show good sintering behaviour and a homogeneous grain and bond microstructure with coarse quartz particles held together by a finer matrix. Internal defects such as cracks or other similar faults were not observed.

The RSM sample (100/0) shows a porous microstructure formed by closed and open pores. Open pores are formed by intercommunicated irregular channels with a size below 5 μm. Their origin lies in the loss of volume associated to the dehydroxylation of clay mineral in firing. In this sample, closed porosity is mainly due to fine closed porosity consisting of small size pores (<10 μm) distributed throughout the ceramic matrix. Moreover, interparticle porosity composed of pores with an irregular morphology at quartz and feldspar grain boundaries with the glassy matrix are also observed. Larger quartz particles can be clearly distinguishable by showing micro-cracks. After their allotropic transformation (573 °C), quartz particles undergo pronounced shrinkage, which increases microscopic stresses. As the piece cools, the particles begin to debond from the matrix, giving rise to peripheral cracks. The addition of ilmenite mud as additive in the RSM paste has a positive effect on the sinterization process. Thus, open

porosity decreases in 97/3 and 95/5 bodies as the ilmenite mud added increase. However, higher additions leads to an opposite effect on the porosity, which begins to increase as the percentage of ilmenite mud in the composition increases. This effect is more noticeable in samples 70/30 and 50/50 in which the volume of irregular intercommunicated channels has increased significantly (see Fig. 8).

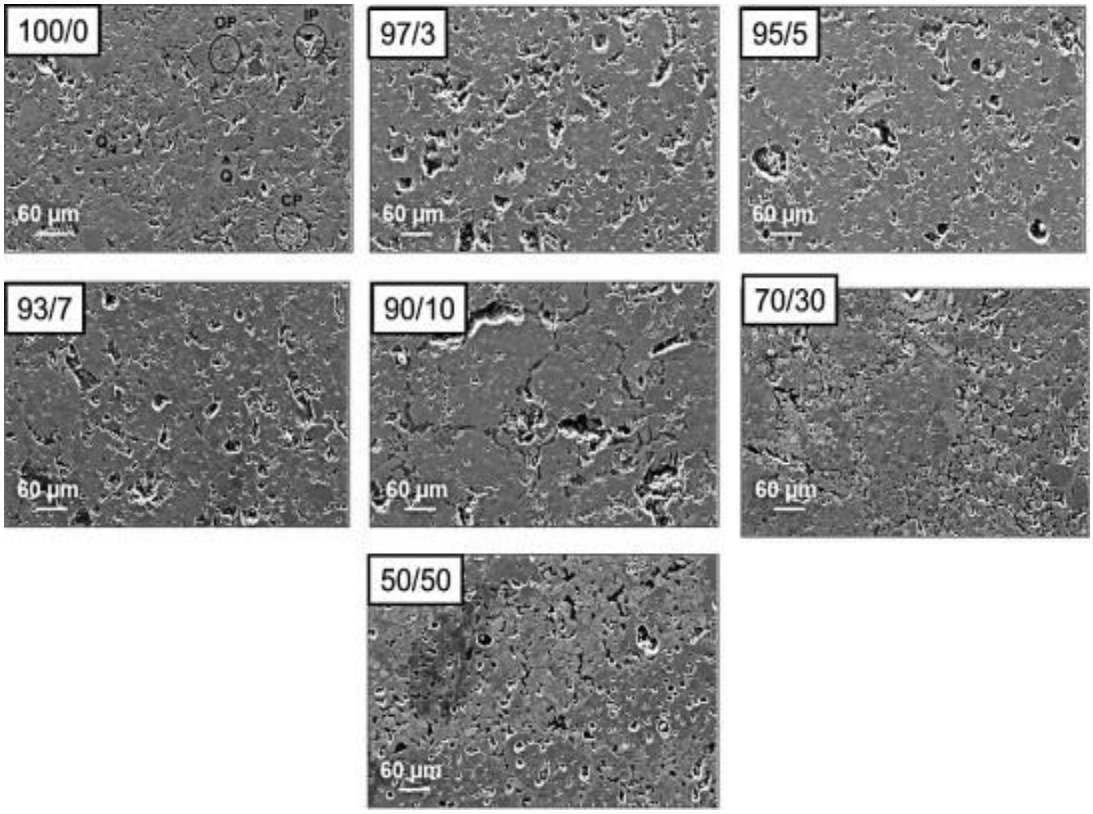

Fig. 7. Secondary electron images (low magnification) on polished surfaces of fired tiles. Q: quartz; OP: open porosity; CP: close porosity and IP: interparticle porosity.

Fig. 9 shows FESEM images together with the elemental mappings of Al, Si, Fe, Ti y Zr in the samples 100/0, 50/50 and 90/10. The different compounds in the samples are clearly identified by colour differences caused by the different concentrations of each ion in the crystalline phases. The microstructure of 100/0 composition consists of quartz particles surrounded by a matrix enriched in Al_2O_3. It is clearly observed the increase in Ti concentration in the samples as the concentration of ilmenite mud in the composition increases. The sample 100/0, which does not present mud added, titanium oxide appears as an isolated impurity. In the micrography is also shown a iron oxide particle, which is present in the composition of RSM being responsible for its red colour. Therefore, sample 90/10 shows a higher heterogeneity and even

more in sample 50/50, showing all the components dispersed in the sample. The titanium concentration distributed throughout the sample increases in sample 90/10 and especially in 50/50, because they shown the highest amount of tionite. Besides, samples which added tionite shown the presence of Zr and a higher content of Fe that in sample 100/0 without tionite addition. On the other hand, the Si and Al concentration decrease in samples according to the addition of tionite.

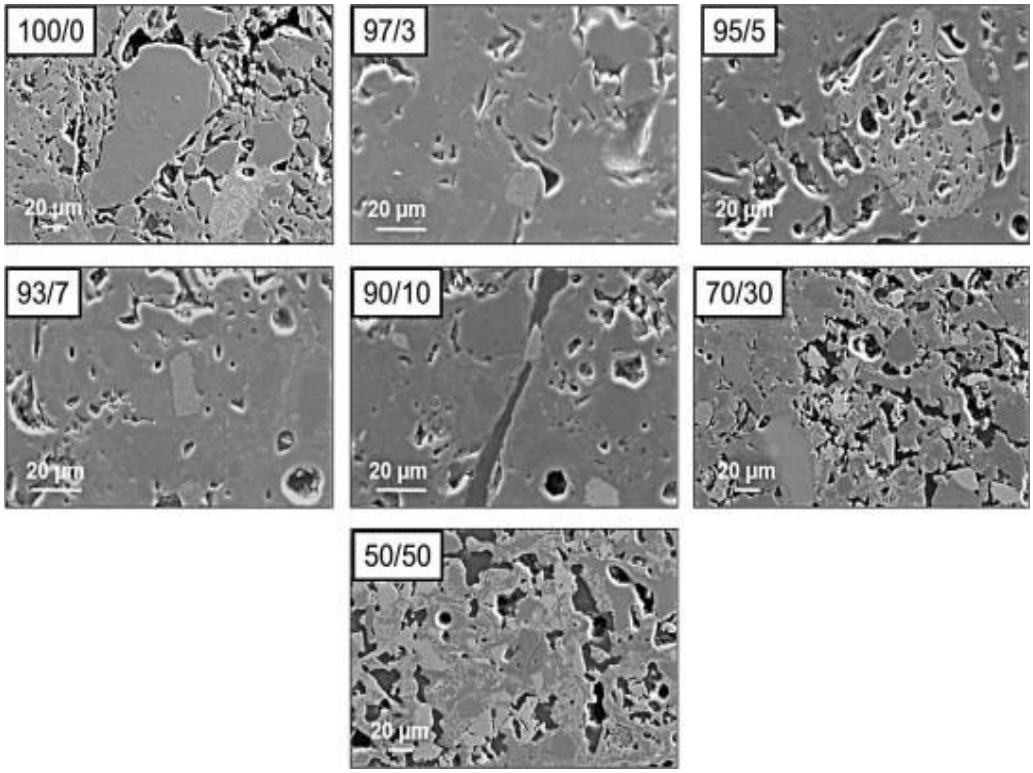

Fig. 8. Secondary electron images (high magnification) on polished surfaces of fired tiles.

3.2. Technological properties of fired tiles

The results shown in Table 3 indicate that the linear shrinkage increases because of the concentration of ilmenite mud also increasing. Lower values are advantageous for traditional ceramics manufacturing because they reduce cracking and volume changes during firing. The linear shrinkage of samples fired at 1150 °C showed values <7%.

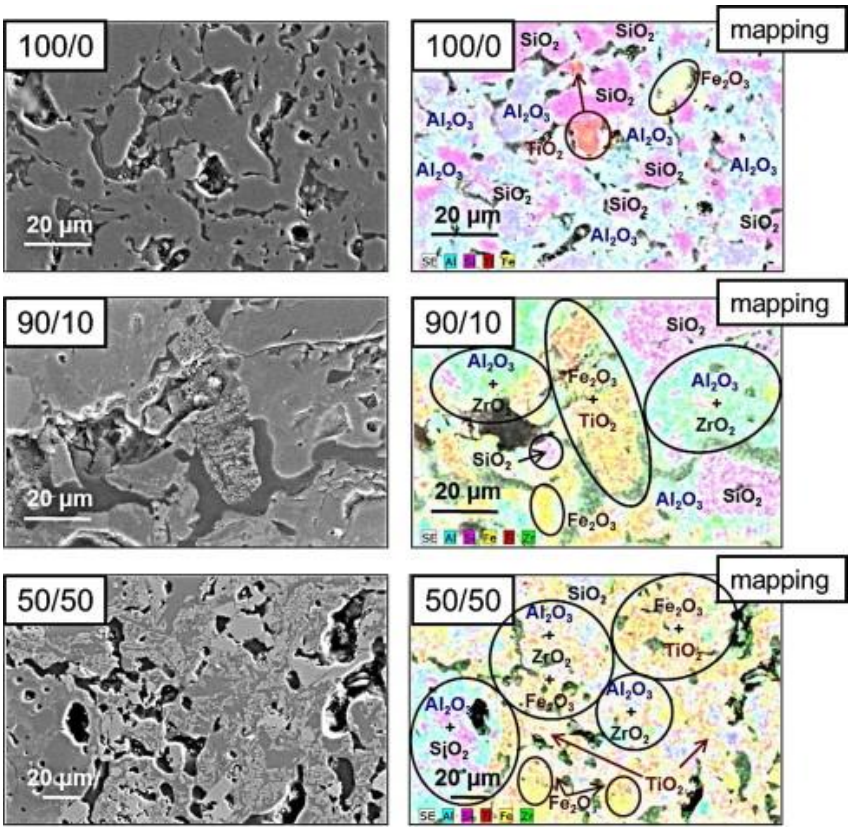

Fig. 9. FESEM images and elemental mappings on polished surfaces of fired 100/0, 50/50 and 90/10 samples.

Table 3. Linear shrinkage and technological properties of fired tiles Results show average values of 10 measurements.

RSM/MUD	Linear shrinkage LS (%)	Apparent porosity P (%)	Water absorption E (wt.%)	Bulk density B (g cm^{-3})	Bending strength BS (MPa)
100/0 (RSM)	3.8 ± 0.1	12.5 ± 0.7	5.30 ± 0.06	2.36 ± 0.02	35.1 ± 0.9
97/3	5.6 ± 0.1	6.71 ± 0.3	2.82 ± 0.05	2.38 ± 0.04	41.1 ± 0.8
95/5	6.0 ± 0.1	5.98 ± 0.2	2.48 ± 0.03	2.42 ± 0.05	40.2 ± 0.8
93/7	6.0 ± 0.1	10.0 ± 0.5	4.18 ± 0.04	2.40 ± 0.03	37.5 ± 0.7
90/10	6.4 ± 0.2	12.0 ± 0.7	4.72 ± 0.06	2.55 ± 0.03	36.5 ± 0.7
70/30	6.3 ± 0.1	19.8 ± 0.8	9.02 ± 0.10	2.22 ± 0.02	33.2 ± 0.8
50/50	6.6 ± 0.1	20.9 ± 0.9	9.18 ± 0.12	2.27 ± 0.05	30.8 ± 0.9

The apparent porosity generally increases with the concentration of ilmenite mud. This physical property is very important, because it is related to the water absorption of the fired products [32]. Therefore the water absorption also follows this trend as the properties are directly related. Water absorption is related mostly to open porosity. Thus, the increase in the volume fraction of irregular intercommunicated channels in 70/30 and 50/50 fired samples produces an increase in the water absorption (Fig. 7 and Fig. 8). In addition, the presence of a few rounded and isolated pores indicates the consistent development of the liquid phase during sintering [33]. Moreover the water absorption decreases with the addition of 3% and 5% of

ilmenite mud (2.82 and 2.48 wt.%, respectively), facilitating the subsequent sintering and drying stages. It confirms the results obtained previously by SEM. In accordance with the European Standard EN 14411 [34] ceramic tiles with water absorption coefficient (E) in the interval $0.5\% < E \leqslant 3\%$ belong to the BI_b group, tiles with $3\% < E \leqslant 6\%$ belong to the BII_a group and those with $6\% < E \leqslant 10\%$ belong to the BII_b group. The low values of water absorption and apparent porosity makes these tiles more resistant to freeze–thaw cycles and stain resistant; and in addition they require less drying time.

The bulk density increases with the concentration of ilmenite mud up to 10% because the density of undissolved mud is 3.7 g cm^{-3}. When it is higher than 30% of mud it decreases radically because of the increase in the porosity.

The bending strength increases as the ilmenite mud percentage increases from 100/0 to 90/10 compositions due to the beneficial effect of ilmenite addition on sintering during firing as denoted by the decrease in porosity. The addition of mud up to 10% lowers the rupture tension because of the porosity increases (Table 3). On the other hand, bending strength values in 70/30 and 50/50 samples decreases; being even lower than that corresponding to the composition 100/0 without addition of ilmenite mud. This result is likely due to the increase in the volume fraction of interconnecting open pores, which act as large fracture flaws reducing bending strength.

In any case, bending strength values for 97/3 and 95/5 composition are upper the minimum value of 30 MPa required in standard EN 14411 for tiles belonging to the BI_b group; the corresponding values for 100/0, 93/7 and 90/10 samples are greater than 22 MPa, which is the minimum value for tiles in the BII_a group and finally, 70/30 and 50/50 composition show bending strength values above the minimum value of 18 MPa required for tiles in the BII_agroup [34].

3.3. Environmental study

3.3.1. Radiological and radioactive characterisation

The original mud had a total radionuclide concentration (2.0–3.0 Bq g^{-1}) that surpassed the 1 Bq g^{-1} EU safety threshold for Naturally Occurring Radioactive Material (NORM) wastes[35]. The radionuclides with the highest activity concentrations are for ^{226}Ra and ^{228}Ra, being them around 500 and 1200 Bq kg^{-1}, respectively [11]. These concentrations are significantly higher than the average worldwide values for soils (25 Bq kg^{-1} of ^{238}U and ^{232}Th in secular equilibrium with their daughters) [36] and [37]. In the mixtures, the activity

concentration of these radionuclides increased with increasing mud content, as did those of ^{228}Ra, ^{228}Th, and ^{238}U. The activity concentration of ^{40}K was constant in all samples.

On the other hand, ^{210}Po was reduced drastically during the firing process (from 300 to 70 Bq kg^{-1}), because of the high volatility of Po above 200 °C [38].

The high radioactive content of the mud samples raises the question of whether this waste can be valorised as building material. In order to evaluate this problem, the European Union has proposed reference values for the natural radionuclide concentrations in building materials [35], defining an external risk index (I), also called activity concentration index, according to the following equation:

$$I = \frac{C^{226}\mathrm{Ra}}{300\ \mathrm{Bq/kg}} + \frac{C^{232}\mathrm{Th}}{200\ \mathrm{Bq/kg}} + \frac{C^{40}\mathrm{K}}{3000\ \mathrm{Bq/kg}} \quad (5)$$

where C^{226}Ra, C^{232}Th, and C^{40}K are the activity concentrations for ^{226}Ra, ^{232}Th, and ^{40}K, respectively, expressed in Bq kg^{-1}.

This index should not exceed the value of unity ($I \leqslant 1$) for materials used in bulk amounts, e.g. concrete, or $I \leqslant 6$ for superficial materials and those with restricted use, e.g. tiles, boards, etc., to ensure that the additional external dose received by occupants living in buildings constructed with these materials does not exceed the reference value of 1 mSv year^{-1} [39].

Table 4 shows that index I is significantly lower than six for all analysed materials. This renders undissolved mud a suitable material for use in the ceramic industry in comparison with other additives [40] and [41].

3.3.2. Radon potential and exhalation rate of matrix and blocks

The radon emanation factor is the fraction of the ^{222}Rn produced by the ^{226}Ra in a sample that reaches the pores of the material. The product of radium concentration per the emanation factor gives the radon potential parameter. The radon potential is a characteristic of the material that is not influenced by the experimental conditions during its determination, and therefore is a suitable parameter for classifying/comparing porous materials in relation to its radon radiological risk [42] and [43].

Table 4. Concentration in Bq kg^{-1} of each ceramics tile obtained and external risk rate "I".

RSM/MUD	^{238}U	^{226}Ra	^{210}Po	^{232}Th	^{228}Ra	^{228}Th	^{40}K	"I"
RSMa	39 ± 2	39 ± 3	37 ± 1	58 ± 3	54 ± 6	63 ± 7	832 ± 45	N.M.
100/0 (RSMb)	35 ± 2	50 ± 1	39 ± 2	60 ± 2	61 ± 2	56 ± 2	1104 ± 16	0.84
97–3	37 ± 2	55 ± 1	34 ± 2	62 ± 2	97 ± 3	84 ± 2	1154 ± 15	1.05
95–5	44 ± 2	72 ± 2	40 ± 2	59 ± 2	127 ± 4	108 ± 3	1182 ± 18	1.27
93–7	40 ± 2	79 ± 2	43 ± 4	59 ± 4	141 ± 5	118 ± 4	1158 ± 23	1.35
90–10	37 ± 2	75 ± 2	41 ± 2	63 ± 5	139 ± 5	112 ± 4	1124 ± 24	1.32
0/100 (MUDb)	31 ± 1	457 ± 19	71 ± 4	78 ± 3	1158 ± 48	1112 ± 46	477 ± 30	7.47
MUDa	34 ± 2	335 ± 15	300 ± 19	72 ± 4	952 ± 43	956 ± 43	428 ± 43	N.M.

N.M. not measured.
a Before firing process.
b After firing process.

According to the study made, and once the samples were analysed it is possible to affirm that the Rn potential (Ω) of the samples are below the limit of detection of the system (<5 Bq kg^{-1}), being the typical value of the radon potential in a typical material engineered as cement of about 10 Bq kg^{-1} [35]. Therefore, we can say that the concentration of Rn in air produced by samples in a standard room (5 m × 5 m × 2 m) in the worst conditions is $C_{Rn}^{Sat} < 4\ Bq\ m^3$, somewhat below the limit of 100 Bq m^3 for new constructions according to the recommendation of the Committee on the Environment of the EEC of 21 February 1990[44] and [45].

3.3.3. Leaching test

A TCLP leaching test was applied to evaluate the potential environmental impact generated by hazardous metals contained in the ceramics tiles. Table 5 shows that increasing the proportion of mud in the mixture decreases the leached metals formed in many cases. Attending to these data is concluded that the firing process makes metal less leachable. On the other hand, the *S* increases slightly as the proportion of ilmenite mud increases, because of the sulphate breakdown during the firing process. As explained in TGA results, at a certain temperature the iron sulphate is decomposed, decreasing significantly the concentration of sulphur due to the emission of SO_2 gas.

The leached metals values are clearly lower than the limits imposed by US EPA [46]; these data indicate that the metal concentrations are below the ecotoxicity limits, and will not have a significant impact when this material is released into the environment.

On the other hand, the liquids fractions obtained in the TCLP test were also analysed the radionuclides contents, in order to gain information in relation with the mobility of them. The concentrations of radionuclides are fairly low (Table 6). Transfer factors demonstrate that almost radionuclides leached out after the firing process. The concentration in the leaching liquid decreases with the proportion of mud, with the exception of ^{210}Po. The concentrations of U-isotopes are of the same order of magnitude as typical ones in continental waters, and for Th-isotopes they are one to two orders of magnitude higher, but we can ensure that their potential radiological impact is negligible [47]. In relation to the behaviour of the different radioelements (U, Th, and Po), it was observed that mobility for U and Th is very similar, whereas for Po it is one order of magnitude lower, which can be justified by the high tendency of Po to be bound onto the particulate material [48].

Table 5. Leachability concentrations of metals (μg L^{-1}) obtained by TCLP test from the raw materials and tiles by ICP-OES. Transfer factor (%) into liquid phase of TCLP.

RSM/MUD	RSMa		100/0 (RSMb)		97/3	95/5	93/7	90/10		0/100 (Mudb)		Muda		Liquid 1	U.S. EPA
	μg L^{-1}	%	μg L^{-1}	%	μg L^{-1}	μg L^{-1}	μg L^{-1}	μg L^{-1}	%	μg L^{-1}	%	μg L^{-1}	%	μg L^{-1}	μg L^{-1}
Ba	500	1.76	570	1.90	400	280	310	310	1.04	40	0.10	<20	<0.08	<20	1,000,000
Al	4000	0.10	8600	0.18	2000	1800	2100	2100	0.05	<100	<0.01	<100	<0.01	<100	–
K	18,3	1.33	10,8	0.73	6900	6600	8600	8800	0.63	4600	0.93	15,9	3.21	2400	–
Mg	1400	0.34	21	4.72	3600	5500	8200	9100	1.36	200	0.05	6500	1.76	<100	–
Mn	1000	5.92	1570	7.02	2260	110	1380	1420	4.94	50	0.05	20	0.02	<10	–
Si	42,2	0.37	29,8	0.26	13,7	5700	15,5	15,6	0.16	3700	0.09	700	0.02	1300	–
As	110	22.0	100	22.2	40	40	60	60	40.0	<30	<4.62	<30	<20.0	<30	5000
Ca	4900	0.83	45,4	7.26	14	10,4	17,7	23,1	4.02	1200	0.23	2400	0.66	<100	–
Cr	200	5.80	230	6.48	200	<20	240	220	3.41	<20	<0.08	<20	<0.04	<20	5000
Fe	2100	0.10	314	11.87	322	1420	304	300	10.93	40	0.01	40	0.01	20	–
Pb	100	5.13	100	3.45	300	20	150	110	3.24	<10	<0.07	<10	<0.07	<10	5000
S	8000	80.0	2000	20.0	3000	4000	5000	5000	50.0	<1000	<10.0	885	184.4	<1000	–
Sr	60	1.11	50	0.86	60	50	40	40	0.71	<10	<0.15	<10	<0.15	<10	–
Ti	<10	0.01	<10	0.01	<10	20	<10	<10	0.01	70	0.01	10	0.01	<10	–
Zn	41	0.31	180	1.29	88	63	122	101	0.75	40	0.44	6	0.07	10	25

Limit values given in the U.S. EPA standard.
N.M. not measured.
Liquid 1 are the fluid extractant used in the TCLP test.
a Before firing process.
b After firing process.

Table 6. Average concentration (mBq L^{-1}) of each sample analysed by alpha spectrometry. Transfer factor (%) in TCLP.

	^{238}U		^{234}U		^{232}Th		^{230}Th		^{210}Po	
RSM/MUD	mBq L^{-1}	%	mBq L^{-1}	%	mBq L^{-1}	%	mBq L^{-1}	%	mBq L^{-1}	%
RSMa	29 ± 3	1.5	36 ± 4	1.8	50 ± 17	1.7	129 ± 28	7.6	7.3 ± 1.9	0.4
100/0 (RSMb)	13 ± 2	0.8	20 ± 3	1.1	37 ± 9	1.2	121 ± 17	6.7	16 ± 3	0.8
97/3	10 ± 2	0.6	10 ± 2	0.5	18 ± 6	0.6	54 ± 10	2.5	12 ± 2	0.7
95/5	4.8 ± 1.4	0.2	6.3 ± 1.7	0.3	33 ± 11	1.0	75 ± 17	3.0	10 ± 2	0.6
93/7	6.3 ± 1.4	0.3	5.1 ± 1.2	0.3	11 ± 4	0.4	24 ± 6	1.3	11 ± 3	0.3
90/10	6.4 ± 1.4	0.4	6.4 ± 1.4	0.4	5.1 ± 1.6	0.2	8.0 ± 2.0	0.4	5.5 ± 0.8	0.3
0/100 (Mudb)	1.9 ± 0.8	0.1	1.4 ± 0.7	0.1	28 ± 11	0.7	91 ± 19	3.6	8.9 ± 1.9	2.5
Muda	2.1 ± 0.7	0.1	5.3 ± 1.2	0.3	37 ± 10	1.0	99 ± 18	4.3	10 ± 3	0.1
Liquid 1	3.9 ± 1.4	N.M.	8.3 ± 2.1	N.M.	4.6 ± 2.6	N.M.	8.0 ± 3.5	N.M.	11 ± 2	N.M.

N.M. not measured.
Liquid 1 is the fluid extractant used in the TCLP test.
a Before firing process.
b After firing proces

Finally, neither ^{226}Ra, ^{228}Ra, nor ^{40}K were detected by gamma spectrometry in the leachates of any tile, leading transfer factor values not detected due to the higher limit of detection of this radiometric technique.

4. Conclusions

The present work has demonstrated that ilmenite mud from the TiO_2 industry can be successfully used in the manufacture of red stoneware ceramic bodies. XRD analysis showed that, in relation to the standard tile, no significant effects on the crystalline phases were observed with the addition of undissolved mud. SEM microstructural analysis showed that composition with less than 10% of waste has a finer fracture surface with fewer defects compared with the reference sample (100/0).

The technological properties of the new tiles obtained by adding the mud waste are comparable, or even better, than the commercial sample taken as reference. We have demonstrated that the addition of this mud as additive (3–5%) has a beneficial role as an agent of the sintering processes, decreasing both apparent porosity and water absorption. This facilitates the drying stage thanks to the decrease in water absorption and improve the resistance to cycles of freeze–thaw and to stains. In relation to the water absorption and bending strength, the different tiles can be classified into the following groups: samples formed by the addition of 3–5% of undissolved mud belong to the BI_a group with a water absorption of $0.5\% < E \leqslant 3\%$ and a minimum value required of bending strength of 30 MPa; tiles produced by the addition of 7–10% of ilmenite mud belong to the BII_a group, which includes tiles with a water absorption of $3\% < E \leqslant 6\%$ and a minimum bending strength of 22 MPa. Higher ilmenite mud additions (30–50%) lead to ceramic tiles that can be classified into the BII_b group, which includes tiles with a water absorption of $6\% < E \leqslant 10\%$ and a minimum bending strength of 18 MPa. In all cases, the tiles produced from ilmenite mud clearly exceed bending strength values required in the corresponding groups.

The leaching tests showed that the mobility of metals and radionuclides in the different mixtures is similar to that of the reference tile. The use of undissolved mud waste in red stoneware ceramic bodies can offer a technological solution to the problems caused by its disposal in controlled landfills.

Our research group has studied other uses of the ilmenite mud as, for example, in the manufacturing of materials for fire isolation in building with better isolation properties, or as additive in cements and concretes. We think that effectively the use of ilmenite mud like additive in ceramic manufacturing could be the best potential application of this waste since its

technological properties are significantly improved, and therefore this commercial application could consume all the ilmenite mud production due to the high amount of ceramic produced in worldwide.

Acknowledgements

This research has been partially supported by the Government of Andalusiás Project "Characterization and modelling of the phosphogypsum stacks from Huelva for their environmental management and control" (Ref.: RNM-6300) and by National Institution of Higher Education, Science, Technology and Innovation of the Republic of Ecuador – (SENESCYT for its acronym in Spanish), Prometeo Project. Dr. M.I. Martín expresses her gratitude for the contract JAE-Doc_08-00032 to the Spanish National Research Council (CSIC), co-financed by the European Social Fund Operational Programme 2007–2013 Adaptability and Employment Multiregional. This is a publication No. 59 from CEIMAR Publication Series.

References

[1] Y. Liu, C. Lin, Y. Wu **Characterization of red mud derived of from a combined Bayer process and bauxite calcination method** J Hazard Mater, 146 (2007), pp. 255–261

[2] E. Deydier, R. Guilet, S. Sarda, P. Sharrock **Physical and chemical characterization of crude meat and bone meal combustion residue: waste or raw material** J Hazard Mater, 121 (2005), pp. 141–148

[3] A. Roy, H.C. Eaton, F.K. Cartledge, M.E. Tlttlebaum **Solidification/stabilization of hazardous waste: evidence of physical encapsulation A** Environ Sci Technol, 26 (1992), pp. 1349–1353

[4] Andres A, Fernandez Gómez N, Rivero Gutiérrez S, Viguri JR. Reusing of waste materials in ceramic: analysis of scientific-technical information. In: Proceedings of the 10th mediterranean congress on chemical engineering; 2005.

[5] R. Caligaris, N. Quaranta, M. Caligaris, E. Benavidez **Non-traditional raw materials in the ceramic industry. (Materias primas no tradicionales en la industria cerámica)** Bol Soc Esp Cerám Vidrio, 39 (2000), pp. 623–626

[6] M. Romero, A. Andrés, R. Alonso, J. Viguri, J.M. Rincón **Sintering behaviour of ceramic bodies from contaminated marine sediments** Ceram Int, 34 (2008), pp. 1917–1924

[7] A.T.M. Alsheyaba, T.S. Khedaywi **Effect of electric arc furnace dust (EAFD) on properties of asphalt cement mixture** Resour Conserv Recycl, 70 (2013), pp. 38–43

[8] F. Puertas, I. García-Díaz, A. Barba, M.F. Gazulla, M. Palacios **Ceramic wastes as alternative raw materials for Portland cement clinker production** Cem Concr Compos, 30 (2008), pp. 798–805

[9] N. Quijornaa, A. Coza, A. Andresa, C. Cheeseman **Recycling of Waelz slag and waste foundry sand in red clay bricks** Resour Conserv Recycl, 65 (2012), pp. 1–10

[10] M.J. Gázquez, J.P. Bolívar, R. García-Tenorio, F. Vaca **Physicochemical characterization of raw materials and co-products from the titanium dioxide industry** J Hazard Mater, 166 (2009), pp. 1429–1440

[11] M.J. Gázquez, J. Mantero, J.P. Bolívar **Physico-chemical and radioactive characterization of TiO_2 undissolved mud for its valorisation** J Hazard Mater, 191 (2011), pp. 269–27

[12] L. Pérez-Villarejo, D. Eliche-Quesada, F.J. Iglesias-Godino, C. Martínez-García, F.A. Corpas-Iglesias **Recycling of ash from biomass incinerator in clay matrix to produce ceramic bricks** J Environ Manage, 95 (2012), pp. S349–S35

[13] T. Aloui, A. Ounis, F. Chaabani **Maastrichtian limestones of Feriana Mountain used in white cement production (Central West Tunisia)** J Am Ceram Soc, 91 (11) (2008), pp. 3704–3713

[14] Tay JH, Show KY. Constructive sludge disposal option converting sludge into innovative civil engineering materials. In: Proceedings of the 7th IAWQ Asia-pacific regional conference, Taipei, Taiwan; 1999. p. 1023–28

[15] E.R. Maddrell **Generalized titanate ceramic waste form for advanced purex reprocessing** J Am Ceram Soc, 84 (5) (2001), pp. 1187–1189

[16] M.J. Gázquez **Characterization and recovery of waste generated in the industry for the production of titanium dioxide (Caracterización y valorización de residuos generados en la industria de producción de dióxido de titanio)** University of Huelva (2010)

[17] T. Chernet **Applied mineralogical studies on Australian sand ilmenite concentrate with special reference to its behaviour in the sulphate process** Min Eng, 12 (1999), pp. 485–495

[18] ISO 10545-3:1997. Ceramic tiles. Part 3: Determination of water absorption, apparent porosity, apparent relative density and bulk density.

[19] ASTM C373-88:1999. Standard test method for water adsorption, bulk density, apparent porosity and apparent specific gravity of fired whiteware products.

[20] EN 843-1:2006. Advanced technical ceramics. Monolithic ceramics. Mechanical properties at room temperature. Part. I: Determination of flexural strength

[21] R.L. Lozano, J.P. Bolívar, E.G. San Miguel, R. García-Tenorio, M.J. Gázquez **An accurate method to measure alpha-emitting natural radionuclides in atmospheric filters: application in two NORM industries** Nucl Instrum Methods A, 659 (2011), pp. 557–568

[22] I. López-Coto, J.L. Mas, J.P. Bolivar, R. García-Tenorio **A short-time method to measure the radon potential of porous materials** Appl Radiat Isot, 67 (2009), pp. 133–138

[23] U.S. EPA **Test methods for evaluating solid waste physical chemical methods, SW-846** U.S. Environmental Protection Agency, Washington [DC] (1997)

[24] M. Contreras, M.J. Gázquez, I. García-Díaz, F.J. Alguacil, F.A. López, J.P. Bolívar

Stabilization and valorisation of ilmenite mud waste for the manufacturing of sulfur polymer cements J Environ Manage, 128 (2013), pp. 625–630

[25] J. Martín-Márquez, J.Ma. Rincón, M. Romero **Effect of microstructure on mechanical properties of porcelain stoneware** J Am Ceram Soc, 30 (2010), pp. 3063–3069

[26] J. Martín-Márquez, J.Ma. Rincón, M. Romero **Effect of firing temperature on sintering of porcelain stoneware tiles** Ceram Int, 34 (2008), pp. 1867–1873

[27] W.D. Kingery **Introduction to ceramics** J. Wiley & Sons Press, New York (1976)

[28] J. Martín-Márquez, A.G. De la Torre, M.A.G. Aranda, J.Ma. Rincón, M. Romero **Evolution with temperature of crystalline and amorphous phases in porcelain stoneware** J Am Ceram Soc, 92 (2009), pp. 229–234

[29] L.A. Pérez-Maqueda, V. Balek, J. Poyato, J.L.J. Pérez-Rodríquez, J. Šubrt, I.M. Bountsewa, *et al.***Study of natural and ion exchanged vermiculite by emanation thermal analysis, TG, DTA and XRD** J Therm Anal Calorim, 71 (2003), pp. 715–726

[30] S.M. Pérez-Moreno, M.J. Gázquez, A.G. Barneto, J.P. Bolívar **Thermal characterization of new fire insulating materials obtained from industrial inorganic wastes from TiO_2 industry** Thermochim Acta, 552 (2013), pp. 114–122

[31] A.J. Souza, B.C.A. Pinheiro, J.N.F. Holanda **Recycling of gneiss rock waste in the manufacture of vitrified floor tiles** J Environ Manage, 91 (2010), pp. 685–689

[32] M. Raigón-Pichardo, G. García-Ramos, P.J. Sánchez-Soto **Characterization of a waste washing solid product of mining granitic tin-bearing sands and its application as ceramic raw material** Resour Conserv Recycl, 17 (2) (1996), pp. 109–124

[33] EN 14411:2003. Ceramic tiles. Definitions, clasifications, characteristics and marking.

[34] Office European Commission Report on Radiological Protection. Principles concerning the natural radioactivity of building materials, Radiation Protection 112. Luxembourg: Official Publications of the European Communities; 1999.

[35] United Nations Scientific Committee on the effects of Atomic Radiation (UNSCEAR) **Sources, effects and risks of ionizing radiation. Report to the General Assembly, with annexes** United Nations, New York (1988)

[36] United Nations Scientific Committee on the effects of Atomic Radiation (UNSCEAR)

Report of the United Nations scientific committee on the effects of atomic radiation United Nations, New York (2000)

[37] H. Mabuchi **On the volatility of some polonium compounds** J Inorg Nucl Chem, 25 (1963), pp. 657–660

[38] McNulty GS. Production of titanium dioxide. Plenary lecture. In: NORM V international conference Seville, Spain; 2007.

[39] K. Kovler **Radiological constraints of using building materials and industrial by-products** Constr Build Mater, 23 (2009), pp. 246–253

[40] K. Kovler, G. Haquin, V. Manasherov, E. Neman, N. Lavi **Limitation of radionuclides concentration in building materials available in Israel** Build Environ, 37 (2002), pp. 531–537

[41] A.F. Maged, F.A. Ashraf **Radon exhalation rate of some building materials used in Egypt** Environ Geochem Health, 27 (2005), pp. 485–489

[42] J.G. Ackers, J.F. Den Boer, P. De Jong, R.A. Wolschrijn **Radioactivity and radon exhalation rates of building materials in The Netherlands** Sci Total Environ, 45 (1985), pp. 151–156

[43] C. Pereira, V.K. Vaidyana, P.J. Jojo, T.V. Ramachandran **Measurement of radon exhalation rate from building materials used in the southwest coastal region of India** Indoor Built Environ, 17 (2008), pp. 472–475

[44] J. Lembrechts, M. Jansse, P. Stoop **Ventilation and radon transport in Dutch dwellings computer modelling and field measurements** Sci Total Environ, 272 (2001), pp. 73–78

[45] F.A. López, M. Gázquez, F.J. Alguacil, J.P. Bolívar, I. García-Díaz, I. López-Coto **Microencapsulation of phosphogypsum into a sulfur polymer matrix: physico-chemical and radiological characterization** J Hazard Mater, 192 (2011), pp. 234–245

[46] U.S. Epa **Test methods for evaluating solid waste – physical chemical methods, SW-846** U.S. Environmental Protection Agency, Washington [DC] (1997)

[47] A. Hierro, J.E. Martín, M. Olías, C. García, J.P. Bolivar **Uranium behaviour during a tidal cycle in an estuarine system affected by acid mine drainage (AMD)** Chem Geol, 342 (2013), pp. 110–118

[48] R.R. Bertil, E. Holm **Polonium-210 and lead-210 in the terrestrial environment: a historical review** J Environ Radioact, 102 (2011), pp. 420–429